

**Correlation functions and emission time  
sequence  
of light charged particles from projectile-like  
fragment source  
in  $E/A = 44$  and  $77$  MeV  $^{40}\text{Ar} + ^{27}\text{Al}$   
collisions**

R. Ghetti<sup>a,1</sup>, and J. Helgesson<sup>b</sup>

<sup>a</sup>*Department of Physics, Lund University, Box 118, SE-221 00 Lund, Sweden*

<sup>b</sup>*School of Technology and Society, Malmö University, SE-205 06 Malmö, Sweden*

G. Lanzanò<sup>c</sup>, E. De Filippo<sup>c</sup>, M. Geraci<sup>c</sup>, S. Aiello<sup>c</sup>,  
S. Cavallaro<sup>d</sup>, A. Pagano<sup>c</sup>, and G. Politi<sup>c</sup>

<sup>c</sup>*Dipartimento di Fisica dell'Università di Catania, Istituto Nazionale di Fisica  
Nucleare, Sezione di Catania, Via S. Sofia 64, I-95123 Catania, Italy*

<sup>d</sup>*Laboratori Nazionali del Sud, Catania, and Dipartimento di Fisica dell'Università  
di Catania, Via S. Sofia 44, I-95123 Catania, Italy*

J. L. Charvet<sup>e</sup>, R. Dayras<sup>e</sup>, E. Pollacco<sup>e</sup>, and C. Volant<sup>e</sup>

<sup>e</sup>*DAPNIA/SPhN, CEA/Saclay, F-91191 Gif-sur-Yvette CEDEX, France*

C. Beck<sup>f</sup>, D. Mahboub<sup>f,+</sup>, and R. Nouicer<sup>f,++</sup>

<sup>f</sup>*Institut de Recherches Subatomiques, UMR7500, CNRS-IN2P3 and Université  
Louis Pasteur, B.P. 28, F-67037 Strasbourg CEDEX 2, France*

---

**Abstract**

Two-particle correlation functions, involving protons, deuterons, tritons, and  $\alpha$ -particles, have been measured at very forward angles ( $0.7^\circ \leq \theta_{lab} \leq 7^\circ$ ), in order to study projectile-like fragment (PLF) emission in  $E/A = 44$  and  $77$  MeV  $^{40}\text{Ar} + ^{27}\text{Al}$  collisions. Peaks, originating from resonance decays, are larger at  $E/A = 44$  than at  $77$  MeV. This reflects the larger relative importance of independently emitted light particles, as compared to two-particle decay from unstable fragments, at the higher beam energy. The time sequence of the light charged particles, emitted from the PLF, has been deduced from particle-velocity-gated correlation functions

(discarding the contribution from resonance decays).  $\alpha$ -particles are found to have an average emission time shorter than protons but longer than tritons and deuterons.

---

+) Present address: University of Surrey, Guildford, Surrey GU2 7XH, UK.

++) Present address: Brookhaven Nat. Lab., Upton, New York, 11973-5000, USA.

PACS number(s): 25.70.Pq, 25.70.Mn

Keywords:  $^{27}\text{Al}(^{40}\text{Ar},x)$ ;  $E = 44$  MeV/nucleon,  $77$  MeV/nucleon; Projectile-Like fragment; Light charged particles; Two-particle correlation function; Resonance decays; Emission time sequence.

<sup>1</sup>Corresponding author. Department of Physics, University of Lund.  
Box 118, S-22100 Lund, Sweden. Tel. +46-(0)46-2227647.  
E-mail address: roberta.ghetti@nuclear.lu.se (R. Ghetti).

## 1 Introduction

Extensive studies have demonstrated that semiperipheral heavy-ion collisions at intermediate energies proceed through a dissipative binary reaction mechanism, characterized by early dynamical emission from an intermediate velocity source, followed by statistical evaporation from an excited projectile-like fragment and from an excited target-like fragment [1–7]. In particular, this is true for the reverse kinematics reaction  $\text{Ar} + \text{Al}$ , investigated by several authors [8–18]. In this paper, we aim to study light charged particle (LCP) emission from the PLF, in  $E/A = 44$  and  $77$  MeV  $^{40}\text{Ar} + ^{27}\text{Al}$  collisions. To this end, we investigate experimental two-particle correlation functions of protons, deuterons, tritons and  $\alpha$ -particles.

From previous investigations, as well as from kinematical reasons, it is well known that semiperipheral collisions are dominated by PLF emission at very forward angles (see, e.g., the study of LCP emission from  $E/A = 60$  MeV  $^{40}\text{Ar} + ^{27}\text{Al}$  collisions presented in Ref. [17]). In the present study, the experimental conditions of low detection thresholds, large dynamic range, fine granularity, and small angular separation between the centers of adjacent detectors, allows us to perform the correlation function analysis in a very forward angular range,  $0.7^\circ \leq \theta_{lab} \leq 7^\circ$ .

Information about the emission times of the different particle types can be deduced from a model-independent analysis of the respective measured correlation functions. In particular, we aim to understand the order of emission of the LCPs from the PLF,

by means of particle-velocity-gated correlation functions of non-identical particles [19–21]. This adds an important and novel piece of information to the picture of the reaction mechanism emerging from previous studies [17,18].

Furthermore, we investigate the relative importance of independent (two-) LCP emission from the PLF, as compared to two-particle decay from unstable fragments emitted in the reaction. This is accomplished by comparing the strength of the corresponding resonance peaks in the correlation function at the two beam energies.

The paper is organized as follows. After a brief description of the experimental setup and event selection criteria (Sec. 2), we present the results from the data analysis of the  $E/A = 44$  and  $77$  MeV  $^{40}\text{Ar} + ^{27}\text{Al}$  collisions. These include LCPs kinetic energy spectra (Sec. 3), correlation functions of identical and non-identical particle pairs (Sec. 4), and particle emission time sequence extracted from the velocity-gated two-particle correlation functions (Sec. 5). Finally, a summary and conclusions are given in Sec. 6.

## 2 Experimental details

The data analyzed in this paper were taken at GANIL in two separate experiments with different beam energies.  $E/A = 44$  and  $77$  MeV  $^{40}\text{Ar}$  pulsed beams impinged on  $200 \mu\text{g}/\text{cm}^2$  thick  $^{27}\text{Al}$  targets. The reaction products were detected by the ARGOS [18] multidetector system, an array of 112 hexagonal  $\text{BaF}_2$  crystals (surface area  $25 \text{ cm}^2$ ) modified into phoswich by means of fast plastic scintillator sheets ( $700$  and  $1900 \mu\text{m}$  thick for the two beam energies, respectively).

ARGOS was placed inside the Nautilus vacuum chamber, with the following geometry (which is illustrated in Fig. 1 of Ref. [18]). A forward wall of 60 elements was placed between  $0.7^\circ$  and  $7^\circ$  in a honeycomb shape at a distance of  $233 \text{ cm}$  from the target (solid angle  $0.03 \text{ sr}$ ). The angular separation between the centers of two adjacent detectors was  $\approx 1.5^\circ$ . A backward wall of 18 phoswich elements was placed between  $160^\circ$  and  $175^\circ$ , at a distance of  $50 \text{ cm}$  from the target. Finally, a battery of 30 phoswich elements was placed in plane, at angles between  $10^\circ$  and  $150^\circ$ , at a distance from the target variable from  $50$  to  $200 \text{ cm}$ . Further details on the experimental setup can be found in Refs. [18,22,23].

Identification of the reaction products was achieved via shape discrimination of the photomultiplier signals and Time-of-Flight technique [18,22]. LCPs ( $Z = 1$  and  $2$ ) were isotopically separated, while fragments with  $Z \geq 3$  were identified in charge. The particle velocity was directly measured by means of Time-of-Flight technique. The experimental thresholds were set to  $2 \text{ cm/ns}$  for  $E/A = 44 \text{ MeV}$ , and to  $3 \text{ cm/ns}$  for  $E/A = 77 \text{ MeV}$ . The  $\text{BaF}_2$  crystals, of variable thickness up to  $10 \text{ cm}$ , stopped protons of energy up to  $200 \text{ MeV}$ .

Two slightly different trigger conditions were implemented in the two experiments. In the 44 MeV experiment, events were recorded each time the in-plane detectors or the backward wall was fired, a minimum total multiplicity of 2 being registered. In the 77 MeV experiment, instead, a coincidence between any two detectors was sufficient to start the data acquisition.

In this analysis, the event selection aims to choose semiperipheral collisions. This is achieved by requiring that the pairs of LCPs ( $p$ ,  $d$ ,  $t$ , and  $\alpha$ ) detected in the forward wall, must be in coincidence with one PLF (any fragment with atomic charge  $3 \leq Z_{PLF} \leq 18$  and velocity within 70% of the beam velocity) also detected in the forward wall<sup>1</sup>. The analysis of particle velocity spectra and of invariant cross-sections presented in Refs. [18,23], indicates that this type of events is associated with semiperipheral binary collisions, where two sources, with velocities close to the initial velocity of the projectile and of the target nuclei, are formed. In addition, the mid-rapidity region is an abundant source of particles [18].

### 3 Kinetic energy distributions of light charged particles

The laboratory kinetic energy distributions of protons, deuterons, tritons, and  $\alpha$ -particles, measured in the  $E/A = 44$  and 77 MeV  $^{40}\text{Ar} + ^{27}\text{Al}$  reactions, are shown in Fig. 1, integrated in the angular range  $0.7^\circ \leq \theta_{lab} \leq 7^\circ$ . The detection energy thresholds correspond to  $\approx 2$  and 5 MeV/nucleon for  $E/A = 44$  and 77 MeV experiment, respectively.

One can notice several qualitative features:

- 1) The spectra are dominated by a dumb-bell structure, displaying a minimum slightly below the beam energy. This behavior is typical of those particles (from the isotropically emitting PLF) that have a velocity component either parallel to PLF movement (higher energy peak) or antiparallel (lower energy peak) [18]. Because of the Coulomb push from the PLF, these particles will have an energy either higher or lower than the beam energy [24].
- 2) In addition to PLF emission, the spectra also contain contributions from an intermediate velocity source and from a target-like source [18].
- 3) The dumb-bell structure in the energy spectra is more pronounced for  $p$  and  $d$  and it is slightly suppressed for  $t$  and  $\alpha$ . This may be expected, since the Coulomb push per particle experienced by an  $\alpha$ -particle is less than half that experienced by a proton (taking into account the mass and charge of the  $\alpha$ -particle, and its larger

---

<sup>1</sup> For the  $E/A = 44$  MeV experiment, an additional particle detected in the plane or in the backward detectors is required, since this condition was implemented in the hardware trigger of that experiment.

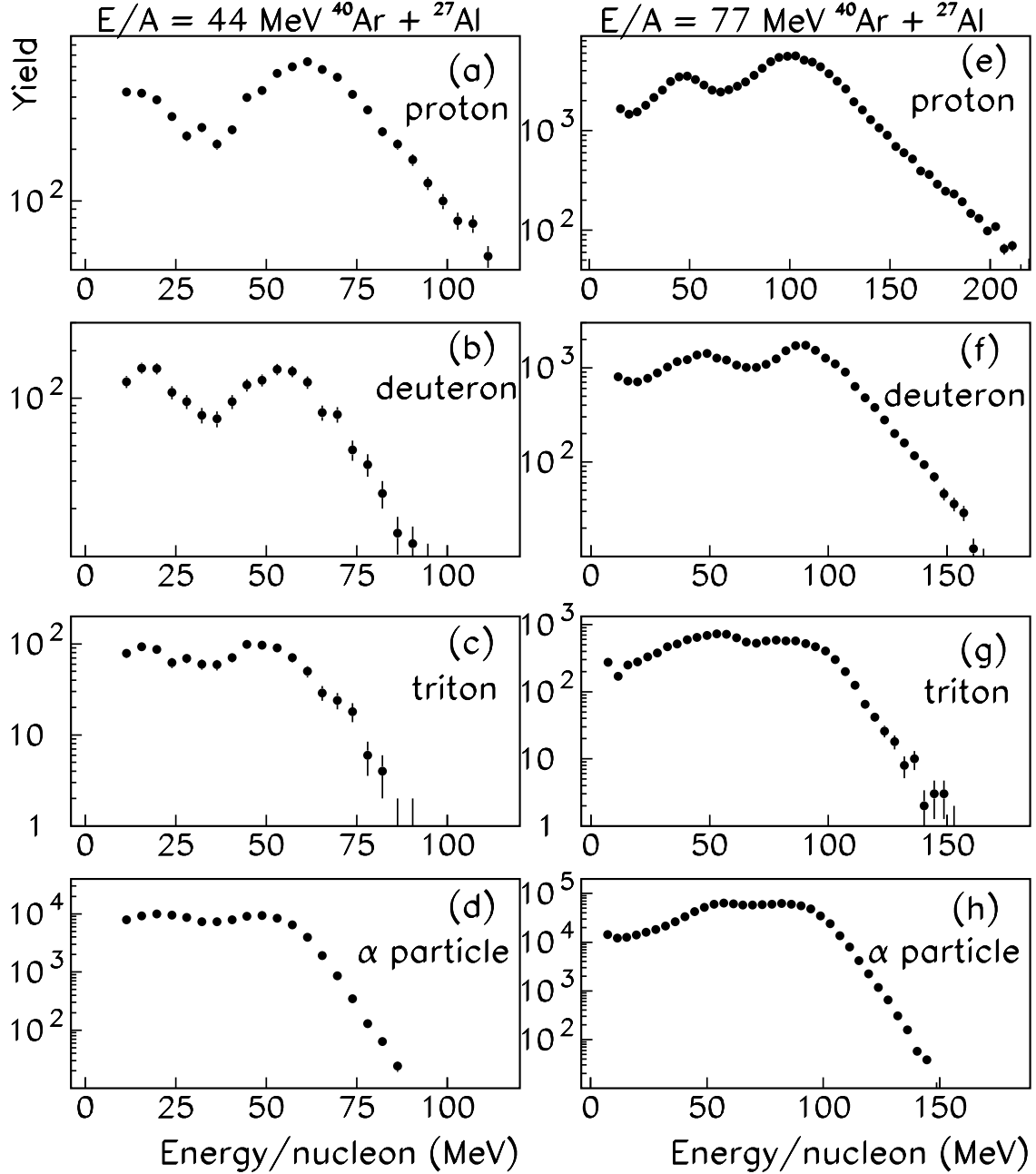


Fig. 1. From  $E/A = 44$  MeV (left column) and  $77$  MeV (right column)  $^{40}\text{Ar} + ^{27}\text{Al}$  collisions, distributions of the laboratory kinetic energy/nucleon of the LCPs detected at  $0.7^\circ \leq \theta_{lab} \leq 7^\circ$ . At a given bombarding energy, all the spectra have the same (arbitrary) normalization.

average emission distance due to its larger size). In addition, the kinematical focusing at forward angles increases with the mass of the emitted particles, and it is strongest for  $\alpha$ -particles [17]. Another effect for the smearing the dumb-bell structure may come from recoil effects. Finally, a reduced dumb-bell shape may be caused by an

enhanced contribution of non-PLF decay mechanisms (such as intermediate velocity source emission and secondary emission from the decay of highly excited primary fragments) for  $t$  and  $\alpha$  emission. Indeed, the average relative intensity of intermediate velocity source emission is larger for  $\alpha$ -particles than for protons, as demonstrated in Ref. [18] for the  $E/A = 44$  MeV  $^{40}\text{Ar} + ^{27}\text{Al}$  reaction.

4) The dumb-bell shape associated with PLF decay is slightly more pronounced at  $E/A = 44$  MeV than at 77 MeV. This is partly explained by the fact that the Coulomb push becomes relatively less important at 77 MeV, as compared to the boost from the source system to the laboratory system. In addition, it may be partly explained by an enhanced contribution of non-PLF decay mechanisms at the higher energy (intermediate velocity source emission and secondary decay) [18,24].

5) The yield of  $\alpha$ -particles is rather large in this forward angular range. Speculations on the origin of these copious  $\alpha$ -particles have been discussed in Refs. [17,18]. It could be due to the production in the reaction of excited light ions, and/or to the  $\alpha$  structure of the two interacting nuclei [25].

#### 4 Two-particle correlation functions

The experimental correlation function is constructed by dividing the coincidence yield,  $N_c$ , by the yield of uncorrelated events,  $N_{nc}$ ,

$$C(\vec{q}, \vec{P}_{tot}) = k \frac{N_c(\vec{q}, \vec{P}_{tot})}{N_{nc}(\vec{q}, \vec{P}_{tot})}. \quad (1)$$

$\vec{q} = \mu(\vec{p}_1/m_1 - \vec{p}_2/m_2)$  is the relative momentum,  $\mu$  is the reduced mass, and  $\vec{P}_{tot} = \vec{p}_1 + \vec{p}_2$  is the total momentum of the particle pair. In the following, an implicit integration over the six variables  $\vec{q}$  and  $\vec{P}_{tot}$  is performed. The correlation function is normalized to unity at large values of  $q$ , where no correlations are expected. The background yield,  $N_{nc}$ , can be constructed either from the product of the singles distributions [26] or with the so-called “event-mixing” technique [27], combining particles from different events. We have verified that, for the present data set, the two techniques yield the same results, within the experimental uncertainty. Thus, we have chosen to utilize the singles technique.

In the present analysis, only particles with energy/nucleon larger than a value slightly below the beam energy have been utilized to construct  $C(q)$ . This is because combining particles from both peaks of the dumb-bell shaped energy distributions (Fig. 1), introduces correlations other than two-body final state interactions and/or quantum symmetrization effects. These unwanted correlations most likely originate from a mixing of sources with different velocities. For more details, see Ref. [24]. By apply-

ing this energy cut, the contribution from the PLF source relative to other sources is enhanced, while the statistics and the accessible range of relative momenta are reduced. Nevertheless, thanks to the small angular separation between the centers of two adjacent detectors ( $\approx 1.5^\circ$ ), the region of small relative momenta (where interesting signatures of final state interactions and antisymmetrization effects appear) is still populated.

Before we proceed to analyze the experimental results, we would like to point out that, for those correlation functions characterized by final state interaction leading to resonances, the resonance peaks may a priori have two different origins [28,29]:

i) From processes where an unstable fragment formed in the reaction decays into the two measured particles. If the secondary decay of a specific fragment produces two particles that are measured in coincidence (like in e.g.  ${}^8\text{Be} \rightarrow \alpha + \alpha$  or  ${}^6\text{Li} \rightarrow \alpha + d$ ), the decay will give rise to a resonance peak in the corresponding correlation function.

ii) From interactions between independently emitted particles. De-excitation of the PLF and secondary decay of excited fragments may produce particles are measured in coincidence. The relative distance for most such pairs will be large (in both space and time) and they will interact weakly. This means that they will give rise to correlation effects mainly at small relative momenta [30].

Figure 2 presents the correlation functions of particle pairs measured in the  $E/A = 44$  and  $77$  MeV  ${}^{40}\text{Ar} + {}^{27}\text{Al}$  experiments. The events are selected with the conditions described in Sec. 2. The low energy thresholds are set to  $35$  MeV/nucleon for the  $E/A = 44$  MeV data, and  $65$  MeV/nucleon for the  $E/A = 77$  MeV data, for the reasons discussed above and in Ref. [24].

#### 4.1 *The pp correlation function*

The *pp* correlation function (normalized in the relative momentum region  $q = 80$ – $100$  MeV/c) is shown in Figs. 2(a,f). This result was already presented in Ref. [24]. It exhibits a shallow maximum at  $q \approx 20$  MeV/c, caused by the attractive *s*-wave interaction between the two protons. The maximum at  $20$  MeV/c may be seen as the resonance peak from the decay of the particle unstable  ${}^2\text{He}$ . The minimum at  $q \rightarrow 0$  MeV/c is due to the interplay between quantum antisymmetrization effects and final state Coulomb repulsion between the two protons [31]. The very weak peak at  $20$  MeV/c indicates that proton emission occurs on a long time scale [31].

#### 4.2 The $p\alpha$ correlation function

The  $p\alpha$  correlation function (normalized in the relative momentum region  $q = 100$ – $150$  MeV/c) is shown in Figs. 2(b,g). The broad peak at  $q \approx 54$  MeV/c is due to the unbound ground state of  ${}^5\text{Li}$  (1.69 MeV above the  $p + \alpha$  threshold,  $\Gamma_{cm} = 1.23$  MeV) [32]. Most probably, the bump contains additional contributions from a background of  $p$  and  $\alpha$ -particles emitted independently from source de-excitation (the large yields of  $p$  and  $\alpha$  [17,18] enhance the probability that two such particles are emitted close enough in time that they will experience strong final state interaction).

The very similar behavior of the two  $pp$  and  $p\alpha$  correlation functions at  $E/A = 44$  and  $77$  MeV, indicates that the characteristics of PLF proton and  $\alpha$ -particle emission are rather independent of the beam energy. As demonstrated by the statistical calculations of Ref. [33], different emitted particles from the PLF are sensitive to different portions of the PLF de-excitation cascade. Because of the Coulomb barrier and of the binding energy relative to the available excitation of the PLF, the emission time distribution of protons and  $\alpha$ -particles is expected to be rather flat. In the calculations of [33], the emission time distribution exhibited by  $\alpha$ -particles is found to decrease by only a factor of 3 over the time interval of 150 fm/c, while other particles (e.g. tritons) exhibit steeper distributions, decreasing more than one order of magnitude in the same time interval. Thus, protons and  $\alpha$ -particles are expected to sample the end of PLF de-excitation cascade, and this effect is expected to be approximately the same at 44 and at 77 A MeV. In addition, there might be a large background of independently emitted protons and  $\alpha$ -particles from secondary decay of excited fragments, also probing the long time scale.

#### 4.3 The $d\alpha$ correlation function

The  $d\alpha$  correlation function (normalized in the relative momentum region  $q = 110$ – $150$  MeV/c) is shown in Figs. 2(c,h). It is governed by the strong resonance at  $q \approx 42.2$  MeV/c, due to the 2.186 MeV ( $\Gamma_{cm} = 0.024$  MeV) excited state of  ${}^6\text{Li}$  [32]. This resonance peak reaches the value  $C(q \approx 42) \approx 4.2$  at  $E/A = 44$  MeV, as compared to  $C(q \approx 42) \approx 2.2$  at  $E/A = 77$  MeV. The resonances expected at  $q \approx 84$  MeV/c and  $102$  MeV/c (from the overlap of the  ${}^6\text{Li}$  excited states at 4.31 MeV,  $\Gamma_{cm} = 1.30$  MeV, and 5.65 MeV,  $\Gamma_{cm} = 1.50$  MeV) [32] are hardly seen in the data.

#### 4.4 The $t\alpha$ correlation function

The  $t\alpha$  correlation function (normalized in the relative momentum region  $q = 180$ – $200$  MeV/c) is shown in Figs. 2(d,i). Because of experimental difficulties in the identification of low energy tritons and  $\alpha$ -particles, the  $t\alpha$  correlation function is presented in



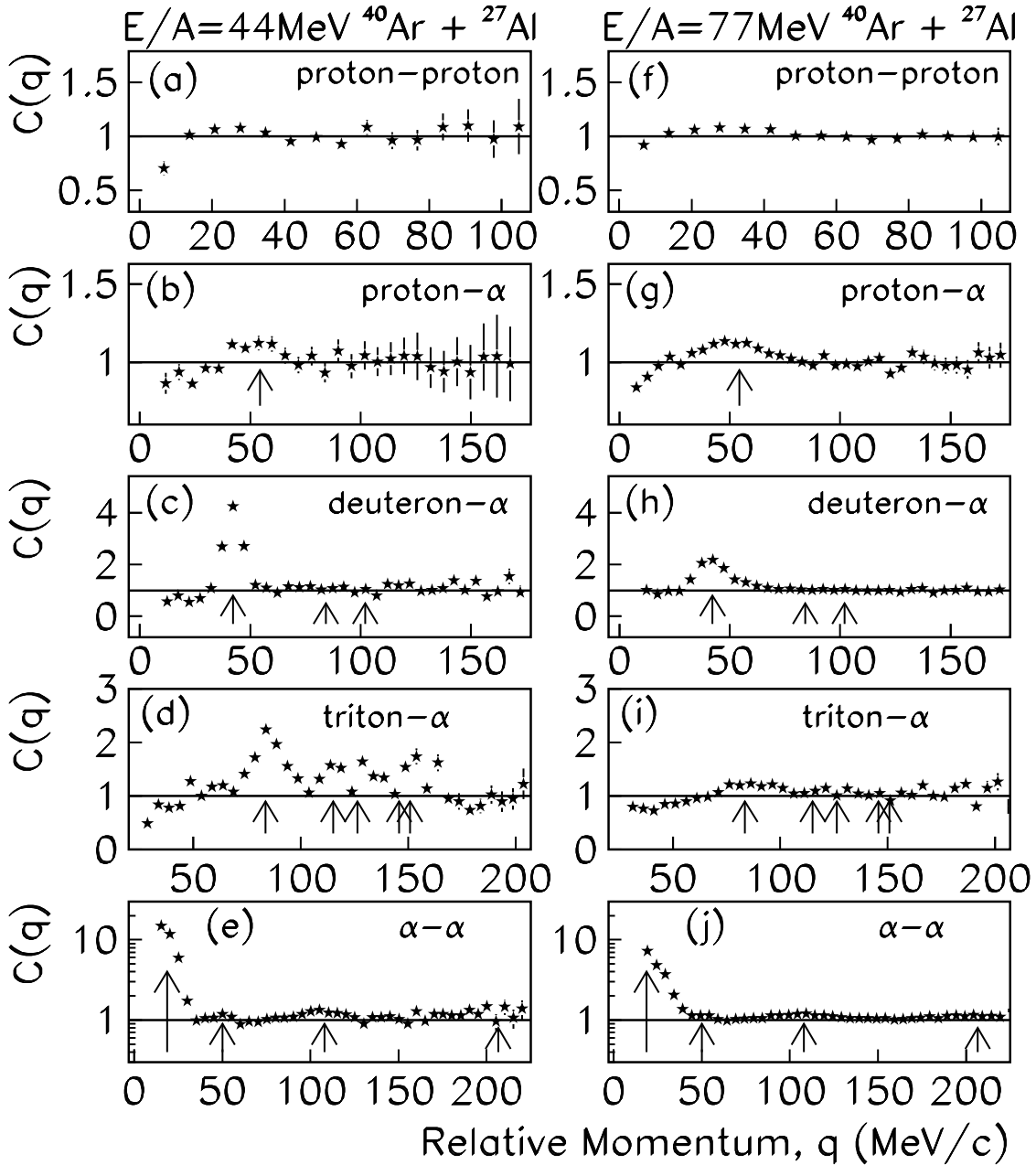


Fig. 2. From  $E/A = 44$  (left column) and  $77$  (right column) MeV  $^{40}\text{Ar} + ^{27}\text{Al}$  collisions,  $pp$  [panels (a,f)],  $p\alpha$  [panels (b,g)],  $d\alpha$  [panels (c,h)],  $t\alpha$  [panels (d,i)], and  $\alpha\alpha$  [panels (e,j)] correlation functions. The position of expected resonance peaks is indicated by the arrows.

the region  $q > 30$  MeV/c [the x-axis scale is zero-suppressed in Figs. 2(d,i)]. The  $t\alpha$  correlation function is characterized by a maximum at  $q \approx 83.6$  MeV/c, due to the 4.652 MeV ( $\Gamma_{cm} = 0.069$  MeV) excited state of  $^7\text{Li}$  [32]. This resonance peak reaches the value  $C(q \approx 83) \approx 2.1$  at  $E/A = 44$  MeV, as compared to  $C(q \approx 83) \approx 1.2$  at  $E/A = 77$  MeV. Other excited states of  $^7\text{Li}$  that decay into  $t\alpha$  are at 6.60 MeV ( $\Gamma_{cm}$

=0.918 MeV), 7.45 MeV ( $\Gamma_{cm} = 0.080$  MeV), 9.09 MeV ( $\Gamma_{cm} = 2.752$  MeV), and 9.57 MeV ( $\Gamma_{cm} = 0.437$  MeV) [32]. The corresponding resonances, expected at  $q = 115.1, 126.3, 145.7,$  and  $150.8$  MeV/c, are visible in the  $E/A = 44$  MeV data.

#### 4.5 The $\alpha\alpha$ correlation function

The  $\alpha\alpha$  correlation function, (normalized in the relative momentum region  $q = 140$ – $180$  MeV/c) is shown in Figs. 2(e,j), in semi-logarithmic scale. This result was already presented in Ref. [24]. This correlation function is dominated by the decay of the particle unstable ground state of  ${}^8\text{Be}$  ( $\Gamma_{cm} = 5.57$  eV) at  $q = 18.6$  MeV/c [34]. This resonance peak reaches the value  $C(q \approx 18) \approx 13.5$  at  $E/A = 44$  MeV, and  $C(q \approx 18) \approx 8.5$  at  $E/A = 77$  MeV. The decay of the 2.43 MeV excited state of  ${}^9\text{Be}$  ( $\Gamma_{cm} = 0.78$  keV) into the undetected neutron and the unstable  ${}^8\text{Be}$  ground-state, as well as the decay of the 3.03 MeV ( $\Gamma_{cm} = 1.51$  MeV) and 11.35 MeV ( $\Gamma_{cm} = 3.5$  MeV) excited states of  ${}^8\text{Be}$  [34], lead to resonance peaks at  $q \approx 50, 108,$  and  $206$  MeV/c, more clearly visible in the  $E/A = 44$  MeV data.

In summary, comparing the results from the two beam energies, we have seen that the resonance peaks are more pronounced at  $E/A = 44$  MeV than at  $77$  MeV. The effect is largest for the  $d\alpha$  correlation function (ratio of main peaks is 1.90), followed by the  $t\alpha$  (ratio of main peaks is 1.75) and the  $\alpha\alpha$  (ratio of main peaks is 1.59). This indicates that at  $E/A = 77$  MeV there is a larger yield of uncorrelated light particles (in particular  $d$  and  $t$ ) as compared to heavy fragments (in particular  ${}^8\text{Be}, {}^7\text{Li},$  and  ${}^6\text{Li}$ ). This finding is in agreement with the results from the analysis of the particle-velocity-gated correlation functions, presented in the next section.

## 5 Particle emission time sequence

Correlation functions of non-identical particles can be utilized to provide information about the order of emission of the different particles [35]. To this end, particle-velocity-gated correlation functions are constructed [19,20].

For non-identical particles, say  $a$  and  $b$ , we construct the correlation functions  $C_a(q)$ , gated on pairs with  $v_a > v_b$ , and  $C_b(q)$ , gated on pairs with  $v_b > v_a$ . If particle  $a$  is emitted later (earlier) than particle  $b$ , the ratio  $C_a/C_b$  will show a peak (dip) in the region of  $q$  where there is a correlation, and a dip (peak) in the region of  $q$  where there is an anticorrelation. The particle velocities are calculated in the frame of the PLF. A single normalization constant, calculated from the ungated correlation function, is utilized for both  $C_a$  and  $C_b$  [20].

The  $p\alpha, d\alpha,$  and  $t\alpha$  correlation functions are characterized by final state interaction

leading to resonances. If the two particles are emitted independently, the velocity-gated correlation functions contain information on the time sequence, but this is not the case if the two particles originate from the decay of an unstable fragment emitted in the reaction. In the latter case, the two particle velocities are determined by momentum conservation, and, in the rest system of the decaying fragment, the lightest particle will always get the highest velocity. Therefore, the expected behavior for particle pairs coming from a two-body decay of a decaying fragment is the following: the velocity-gated correlation function, obtained with the condition that the lightest particle has the largest velocity, should exhibit the strongest correlation or anticorrelation. Therefore, when we, in some cases, observe the opposite behavior (namely that the gate where *the heaviest* particle has the largest velocity leads to a stronger correlation or anticorrelation) we can reliably conclude that this behavior is dominated by a mechanism different than two-body decay. We attribute this effect to the interaction of independently emitted particles, and, in this case, we use the velocity-gated correlation function to obtain information on the time sequence of the independently emitted particles [36].

### 5.1 *The particle-velocity-gated $p\alpha$ correlation function*

The particle-velocity-gated  $p\alpha$  correlation function is shown in Fig. 3. In the relative momentum region dominated by the two-body decay of  ${}^5\text{Li}$  ( $q \approx 54$  MeV/c) the enhancement of  $C_p$  ( $v_p > v_\alpha$ ) over  $C_\alpha$  ( $v_\alpha > v_p$ ), expected from momentum conservation, is not observed. This is a first indication that the behavior of the  $p\alpha$  correlation function is dominated by a background of independently emitted pairs.

The emission chronology can be deduced from the behavior at  $q < 30$  MeV/c, where there are no resonant states that directly lead to the formation of  $p\alpha$  pairs, and where the  $p\alpha$  correlation function displays an anticorrelation ([37] and Fig. 2). The fact that pairs with  $v_p > v_\alpha$  (contributing to  $C_p$ ) interact more strongly (stronger anticorrelation at  $q < 30$  MeV/c) indicates that, on average, protons are emitted later than  $\alpha$ -particles. Inspection of the  $C_p/C_\alpha$  ratios (Fig. 3, lower panels) reveals that the deduced  $p\alpha$  emission chronology is qualitatively similar for the two beam energies.

### 5.2 *The particle-velocity-gated $d\alpha$ correlation function*

The particle-velocity-gated  $d\alpha$  correlation function is shown in Fig. 4. For  $d\alpha$  pairs, the behavior of the  $C_d/C_\alpha$  ratio (Fig. 4 lower panels) is of delicate interpretation, being dominated by the two-body resonance decays of  ${}^6\text{Li}$ . For  $d\alpha$  pairs originating from the two-body decay of  ${}^6\text{Li}$  excited states, the inequality  $v_d > v_\alpha$  should hold in the  ${}^6\text{Li}$  rest system (due to momentum conservation), leading to an enhancement

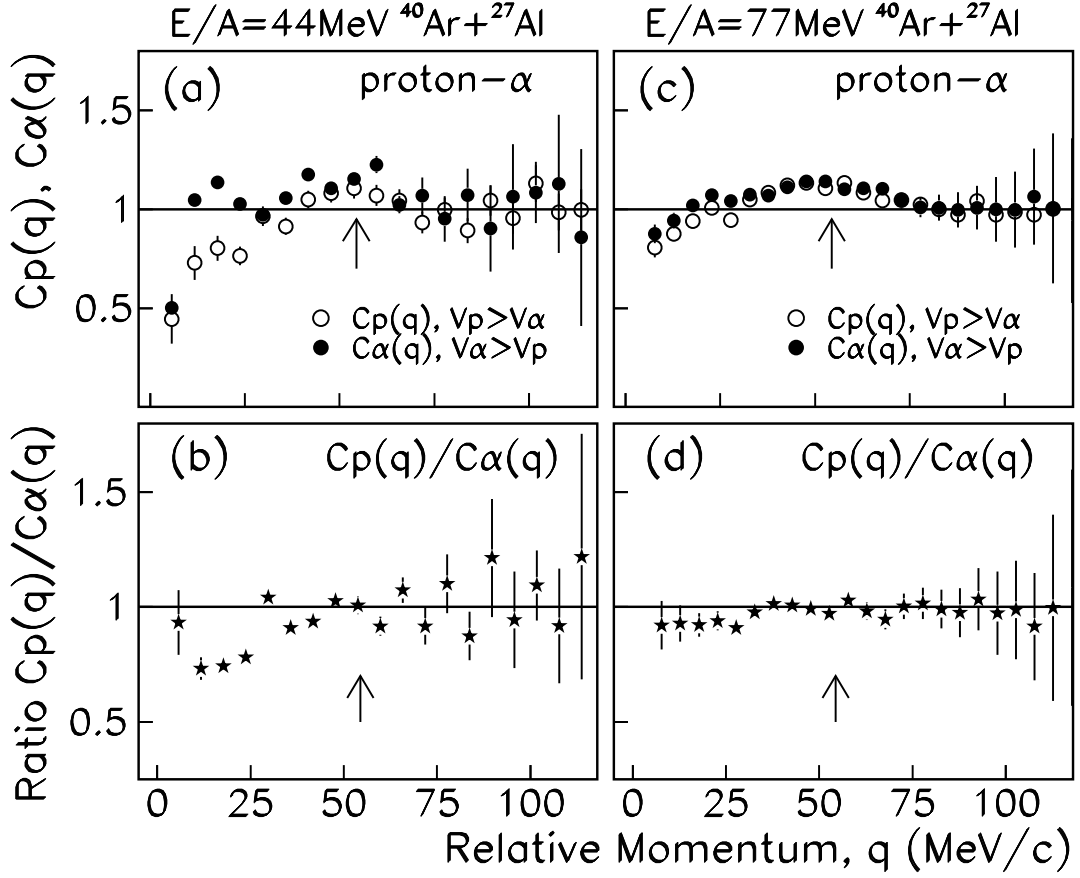


Fig. 3. From  $E/A = 44$  MeV (left column) and 77 MeV (right column)  $^{40}\text{Ar} + ^{27}\text{Al}$  collisions, upper panels: particle-velocity-gated (filled and open circles)  $p\alpha$  correlation functions; lower panels: the ratio of the particle-velocity-gated correlation functions.

of the  $C_d$  correlation function in the PLF system at  $q \approx 42.2$  MeV/c (as discussed above).

The experimental data display such an enhancement of the  $C_d$  correlation function in the  $E/A = 44$  MeV measurement [Fig. 4(a)], therefore it is difficult to deduce the emission chronology in this case. To this end, one has to rely on the behavior of the particle-velocity-gated correlation function at  $q < 30$  MeV/c, where there are no resonant states and where the  $d\alpha$  correlation function displays an anticorrelation [37]. However, the statistics is very low in this region. Nevertheless, the fact that pairs with  $v_\alpha > v_d$  interact more strongly [the ratio  $C_d/C_\alpha$  is larger than unity in this anticorrelation region, Fig. 4(b)] gives an indication that deuterons are, on average, emitted earlier than  $\alpha$ -particles.

The kinematical signature of two-body resonance decay is much weaker in the  $E/A = 77$  MeV  $d\alpha$  data. The enhancement of  $C_d$  over  $C_\alpha$  is not observed [Fig. 4(c)], and the

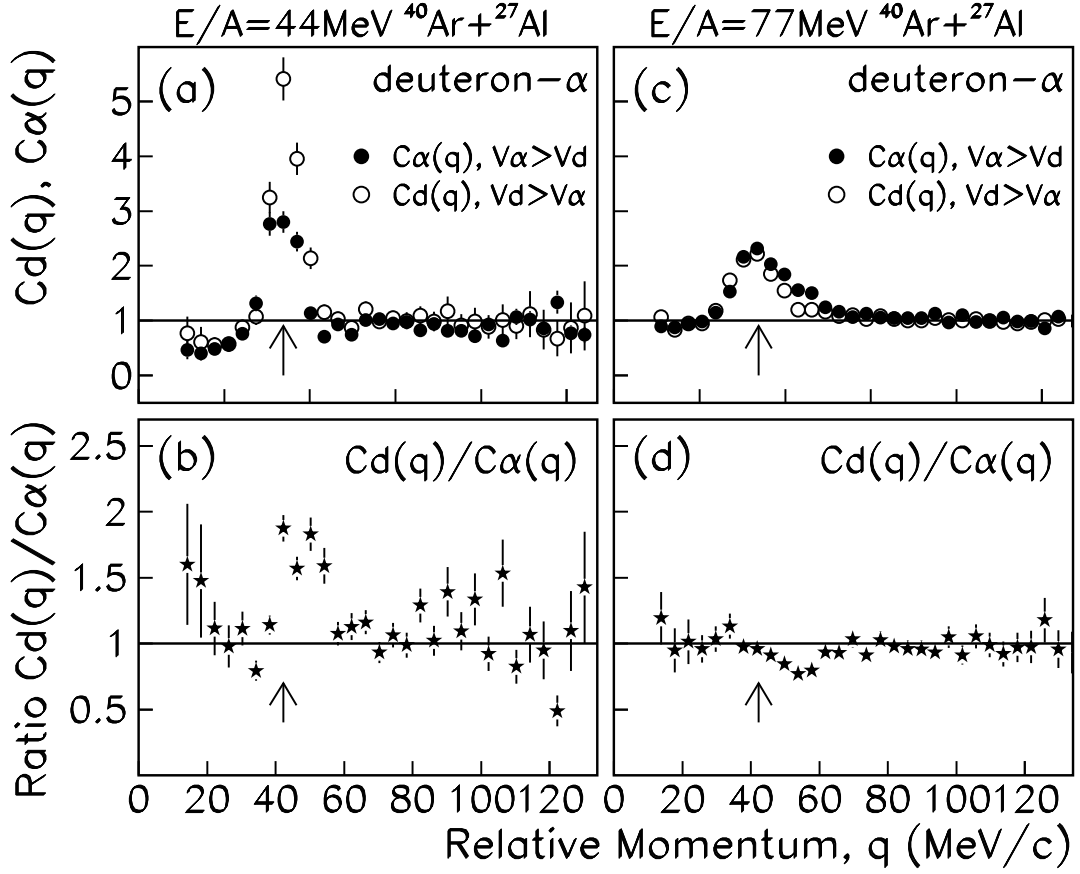


Fig. 4. From  $E/A = 44$  MeV (left column) and 77 MeV (right column)  $^{40}\text{Ar} + ^{27}\text{Al}$  collisions, upper panels: particle-velocity-gated (filled and open circles)  $d\alpha$  correlation functions; lower panels: the ratio of the particle-velocity-gated correlation functions.

ratio  $C_d/C_\alpha$  is close to unity at  $q \approx 42.2$  MeV/c [Fig. 4(d)], while it exhibits a dip in the region  $q \approx 40$ – $70$  MeV/c, where the  $d\alpha$  correlation function displays a correlation [37]. Such a dip cannot originate from the decay of  $^6\text{Li}$  (for momentum conservation reasons, see previous discussion). This indicates that the yield of  $d\alpha$  pairs measured at  $E/A = 77$  MeV is largely contributed by pairs that are not emitted by the decay of  $^6\text{Li}$  excited states, but that are emitted independently from PLF or secondary fragment decay.

The fact that  $C_\alpha$  shows a stronger correlation than  $C_d$ , reflects that the average effective distance between the two particles is smaller for  $C_\alpha$  than for  $C_d$ . Since for  $C_\alpha$ ,  $v_\alpha > v_d$ , this is only possible if (the slower) deuterons are on average emitted before (the faster)  $\alpha$ -particles. Thus, the result of the emission time chronology for these pairs, as deduced from the dip in the  $C_d/C_\alpha$  ratio at  $q \approx 40$ – $70$  MeV/c, is that deuterons are, on average, emitted earlier than  $\alpha$ -particles.

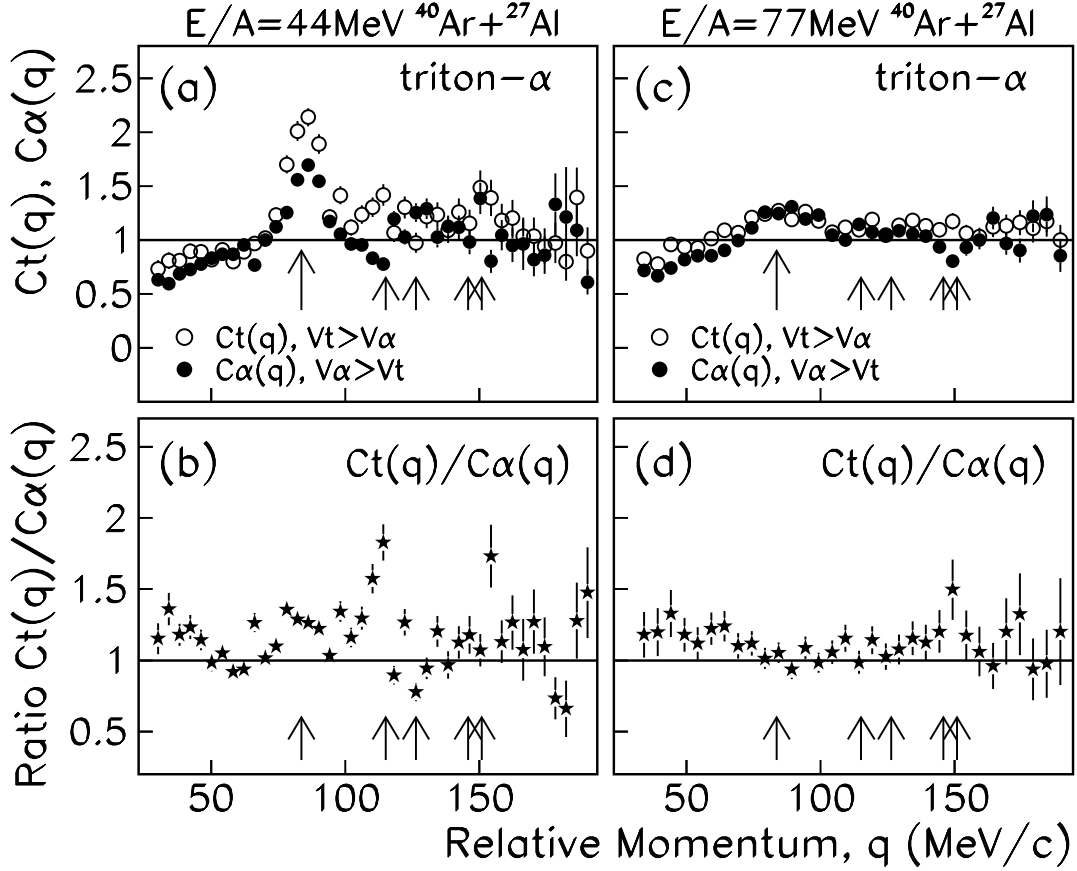


Fig. 5. From  $E/A = 44$  MeV (left column) and 77 MeV (right column)  $^{40}\text{Ar} + ^{27}\text{Al}$  collisions, upper panels: particle-velocity-gated (filled and open circles)  $t\alpha$  correlation functions; lower panels: the ratio of the particle-velocity-gated correlation functions.

### 5.3 The particle-velocity-gated $t\alpha$ correlation function

The particle-velocity-gated  $t\alpha$  correlation function is shown in Fig. 5. Also in this case, the resonance peaks are more pronounced at  $E/A = 44$  MeV than at 77 MeV. For the  $E/A = 44$  MeV data, the behavior of the  $C_t/C_\alpha$  ratio at  $q > 70$  MeV/c is dominated by the kinematical signature of these two-body decays. Due to momentum conservation, the inequality  $v_t > v_\alpha$  dominates in the PLF frame for  $t\alpha$  pairs originating from two-body decays, leading to an enhancement of the particle-velocity-gated correlation function  $C_t$ .

The emission chronology is deduced from the behavior of the particle-velocity-gated correlation function at  $q < 70$  MeV/c, where there are no resonant states and the  $t\alpha$  correlation function displays an anticorrelation ([37] and Fig. 2). For both  $E/A = 44$  and 77 MeV data, this anticorrelation is stronger for  $C_\alpha$  (i.e. the ratio  $C_t/C_\alpha$  is larger

than unity in this anticorrelation region, see Fig. 5, lower panels). Following the same kind of reasoning discussed above, this indicates that tritons are, on average, emitted earlier than  $\alpha$ -particles.

In summary, the results from the analysis of particle-velocity-gated correlation functions indicate that, at both bombarding energies,  $\alpha$ -particles have an average emission time shorter than protons, but longer than deuterons and tritons. As we have pointed out, because of the dominating behavior of the resonant states at  $E/A = 44$  MeV (discussed in Sec. 4), the study of the particle emission chronology from the analysis of particle-velocity-gated  $d\alpha$  and  $t\alpha$  correlation functions is rather delicate at  $E/A = 44$  MeV. Nevertheless, the indications from the resonance-free, low- $q$  regions, support a particle emission time sequence in agreement with that deduced at the higher bombarding energy.

## 6 Summary and conclusions

Single particle energy spectra and two-particle correlation functions have been measured simultaneously and in coincidence with forward emitted fragments from  $E/A = 44$  and 77 MeV  $^{40}\text{Ar} + ^{27}\text{Al}$  reactions. The measurements have been performed at very forward angles,  $0.7^\circ \leq \theta_{lab} \leq 7^\circ$ , with the aim to study the characteristics of de-excitation of the PLF source.

A signature of PLF decay is found in the energy spectra of protons, deuterons, tritons and  $\alpha$ -particles. These are characterized by a dumb-bell peak structure, originating from those particles, from the isotropically emitting PLF, that have a velocity component either parallel to PLF movement (higher energy peak) or antiparallel (lower energy peak). In order to exclude correlations other than final state interactions and quantum symmetrization effects, only particles from the higher energy peak have been considered, thus enhancing PLF emission [24].

The  $pp$  correlation function indicates a lack of final state interaction, typical of particles emitted by a long-lived source. This feature is found in both  $E/A = 44$  and 77 MeV data, pointing to characteristics of the PLF emission source that are rather independent of the beam energy, for what concerns the long-time tail of the PLF de-excitation chain, probed by protons.

The correlation functions dominated by resonances ( $d\alpha$ ,  $t\alpha$ , and  $\alpha\alpha$ ) consistently display higher resonance peaks at  $E/A = 44$  MeV than at 77 MeV. This indicates that the relative abundance of light particles (in particular  $d$  and  $t$ ) as compared to heavy fragments (in particular  $^8\text{Be}$ ,  $^7\text{Li}$ , and  $^6\text{Li}$ ) is larger at  $E/A = 77$  MeV than at  $E/A = 44$  MeV.

The correlation functions of non-identical particle pairs have been utilized to deduce

the particle emission time sequence in a model independent way, based on particle-velocity-gated correlation functions.

For correlation functions characterized by final state interaction leading to resonances, care has to be taken to deduce information on the emission time sequence from independently emitted particles (discarding particles coming from resonance decays). This can be achieved in two ways:

- i) With particle-velocity gates in regions of relative momentum where there are no resonant states that directly lead to the formation of the particle pair.
- ii) With particle-velocity gates in regions of the relative momentum where there is a resonance peak, but the peak is not dominated by particles coming from resonance decay. When a resonance peak is dominated by particles coming from resonance decay, momentum conservation implies that the correlation is stronger for the particle-velocity-gated correlation function with the velocity of the lighter particle larger than the velocity of the heavier particle. Violation of this condition is a signature that the peak is dominated by independently emitted particles, and can thus be utilized to deduce the particle emission time sequence.

The results from the particle-velocity-gated correlation function analysis indicate that, at both bombarding energies,  $\alpha$ -particles have an average emission time shorter than protons but longer than deuterons and tritons. This finding is consistent with the emerging picture of a PLF that is de-excited by early emission of tritons and deuterons followed by  $\alpha$ -particles and protons. Indeed, because of the Coulomb barrier and of the binding energy relative to the available excitation of the PLF, the emission time distribution of protons and  $\alpha$ -particles is expected to be less steep than that of  $d$  and  $t$  [33].

The deduced LCP emission time sequence appears to be in qualitative agreement with previous experimental findings from three-moving source fits to single particle energy spectra in  $E/A = 44$  and  $60$  MeV  $^{40}\text{Ar} + ^{27}\text{Al}$  collisions [17,18]. The PLF source temperatures deduced from these fits were found to be lowest for protons (3.6 MeV at 44 A MeV, 4.9 MeV at 60 A MeV), followed by  $\alpha$ -particles (4.7 MeV at 44 A MeV, 6.9 MeV at 60 A MeV), then deuterons (5.0 MeV at 44 A MeV, 8.5 MeV at 60 A MeV) and tritons (5.9 MeV at 44 A MeV, 8.5 MeV at 60 A MeV). These findings were interpreted as a suggestion that an important fraction of  $\alpha$ -particles is emitted in the final stage of the collision. Different hypotheses have been advanced to explain this late emission of  $\alpha$ -particles, including the concept of  $\alpha$ -clusterization of nuclei [25] and the production of  $\alpha$ -particles by secondary decay of light fragments produced in the collisions [38,39].

The qualitative interpretations of the data analysis given in the present paper should be supported by comparisons to statistical model calculations. Such model comparisons will be presented in a forthcoming paper [36].



## ACKNOWLEDGEMENTS

Financial support from the Swedish Research Council (Contracts No. F 620-149-2001 and 621-2002-4609), and from “Istituto Nazionale di Fisica Nucleare, Sezione di Catania”, is acknowledged.

## References

- [1] W. U. Schroder, Nucl. Phys. **A 538** (1992) 439c.
- [2] R. Bougault, *et al.*, Nucl. Phys. **A 587** (1995) 499.
- [3] Y. Larochelle, *et al.*, Phys. Lett. B **352** (1995) 8.
- [4] M. F. Rivet, *et al.*, Phys. Lett. B **388** (1996) 219.
- [5] J. F. Lecomte, *et al.*, Phys. Lett. B **387** (1996) 460.
- [6] W. Skulski, *et al.*, Phys. Rev. C **53** (1996) R2594.
- [7] O. Dorvaux, *et al.*, Nucl. Phys. **A 651** (1999) 225.
- [8] R. Dayras, *et al.*, Nucl. Phys. **A 460** (1986) 299.
- [9] R. Dayras, *et al.*, Phys. Rev. Lett. **62** (1989) 1017.
- [10] K. Hagel, *et al.*, Phys. Lett. B **229** (1989) 20.
- [11] J. Péter, *et al.*, Nucl. Phys. **A 519** (1990) 127.
- [12] J. Péter, *et al.*, Nucl. Phys. **A 593** (1995) 95.
- [13] Ph. Eudes, *et al.*, Phys. Rev. C **56** (1997) 2003.
- [14] J. C. Angélique, *et al.*, Nucl. Phys. **A 614** (1997) 261.
- [15] R. Ghetti, *et al.*, Phys. Rev. Lett. **91** (2003) 092701.
- [16] V. Avdeichikov, *et al.*, Nucl. Phys. **A 736** (2004) 22.
- [17] G. Lanzaò, *et al.*, Phys. Rev. C **58** (1998) 281.
- [18] G. Lanzaò, *et al.*, Nucl. Phys. **A 683** (2001) 566.
- [19] R. Lednický, *et al.*, Phys. Lett. **B373** (1996) 30.
- [20] R. Ghetti, *et al.*, Phys. Rev. Lett. **87** (2001) 102701; Phys. Rev. C **70** (2004) 034601.
- [21] D. Gourio, *et al.*, Eur. Phys. J. A **7** (2000) 245.
- [22] G. Lanzaò, *et al.*, Nucl. Inst. Meth. A **312** (1992) 515.
- [23] M. Geraci, Doctoral thesis, Università di Catania 1997 (unpublished).

- [24] R. Ghetti, *et al.*, Phys. Rev. C **70** (2004) 027601.
- [25] P. E. Hodgson and E. Betak, Phys. Rep. **374** (2003) 1.
- [26] F. Zarbakhsh, *et al.*, Phys. Rev. Lett. **46** (1981) 1268.
- [27] G. I. Kopylov, Phys. Lett. B **50** (1974) 472.
- [28] J. Pochodzalla, *et al.*, Phys. Rev. C **35** (1987) 1695.
- [29] P. A. DeYoung, *et al.*, Phys. Rev. C **39** (1989) 128; Phys. Rev. C **41** (1990) R1885, and references therein.
- [30] G. Verde, *et al.*, Phys. Rev. C **65** (2002) 054609.
- [31] S. E. Koonin, Phys. Lett. B **70** (1977) 43.
- [32] D. R. Tilley, *et al.*, Nucl. Phys. A **708** (2002) 3.
- [33] S. Hudan, *et al.*, nucl-ex/0308031 (2003).
- [34] D. R. Tilley, *et al.*, Nucl. Phys. A **745** (2004) 155.
- [35] R. Kotte, *et al.*, Eur. Phys. J. A **6** (1999) 185.
- [36] J. Helgesson, *et al.*, in preparation.
- [37] D. H. Boal and J. C. Shillcock, Phys. Rev. C **33** (1986) 549.
- [38] G. Lanzanò, *et al.*, *Nuclear Physics at GANIL 1994-1995, A Compilation*, edited by M. Bex and J. Galin (Ganil, Caen, 1994-95), 252.
- [39] G. Lanzanò, *et al.*, *Proceedings of the XXXV International Winter Meeting on Nuclear Physics, Bormio, Italy*, edited by I. Iori (Univ. degli Studi di Milano, Milano, 1997) 536.